Innovative Electrode Design for High-Voltage Electrochemical Applications Featuring a Non-Uniform Electric Field Distribution

Supawud Nedphokaew[1] and Nattachote Rugthaicharoencheep[1,*]

ARTICLE INFO

Article history:
Received: 12 January 2024
Revised: 26 March 2024
Accepted: 4 May 2024
Online: 30 June 2025

Keywords:
High-voltage
Ozone generation
Electrode
Medical field
Electric field
Non-uniform

ABSTRACT

This paper presents an innovative electrode design tailored for high-voltage electrochemical applications, characterized by a non-uniform electric field distribution. The objective is pinpoint the configuration and location for generators of ozone gas. Ozone is notable for being free from synthetic chemicals, breaking down quickly within 20 minutes, and leaving no traces in either water or the surrounding environment. This study systematically investigates a range of electrode configurations used in ozone generator systems, enabling a thorough comparative analysis of their performance. Through the application of advanced programming methods, the research critically evaluates the effectiveness and appropriateness of each electrode type, aiming to identify the most efficient designs for ozone production. In addition, the study analyzes the electric field distribution associated with each configuration, allowing for precise control over ozone output. This optimization holds considerable importance in medical contexts, particularly for applications involving the destruction of pathogens and the removal of toxic substances.

INTRODUCTION

Ozone gas (O_3) is produced when oxygen molecules (O_2) encounter high-energy sources such as ultraviolet (UV) radiation or electrical discharges, including phenomena like lightning (Figure 1). Known for its exceptional oxidative capabilities, ozone is among the most powerful oxidizing agents permitted for use today. It demonstrates approximately 51% greater efficacy than chlorine gas and operates over three times faster in neutralizing microorganisms. Ozone disrupts microbial integrity by reacting with organic components within bacterial membranes, causing structural breakdown and subsequent cell death. Its broad-spectrum reactivity allows it to interact effectively with both organic and inorganic materials, enhancing its utility in biotransformation and decomposition processes.

Ozone's powerful oxidative mechanism enables it to convert various organic compounds into harmless end products like carbon dioxide and water. Depending on exposure time and concentration levels, ozone proves highly effective in eliminating a wide array of pathogens—including bacteria, viruses, spores, molds, mildew, mucus, amoebae, and even cyst-form microorganisms [1]. This forms the basis of our in-depth investigation into ozone's disinfection potential and its role in microbial eradication.

This study focuses on analyzing electric field stresses within electrode configurations used in ozone generation systems tailored for sterilization purposes. The core objective is to gain insights into the underlying mechanisms of ozone generation [2], with particular attention to exploiting its chemical reactivity for maximal pathogen destruction. By applying high-voltage electrodes, the system aims to produce sufficient ozone concentrations for effective use in sterile environments, such as clean rooms [3]-[4].

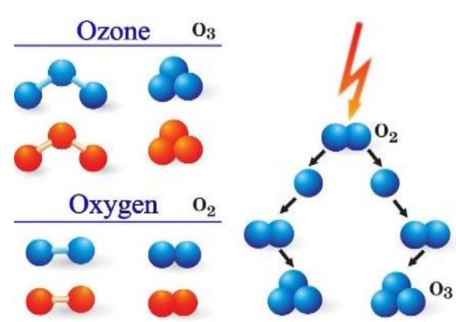

Fig. 1. Ozone generation and pollution removal.

In the past, there was research on electric field such as in 2014 Pramuk Unahalekhaka and Siamrat Phonkaphon studied type 52-3 suspension insulators of 115 kV system of the Provincial Electricity Authority of Thailand. This research studied electric field. Finite Element Analysis

[1]*Department of Electrical Engineering, Faculty of Engineering, Rajamangala University of Technology Phra Nakhon,10800.,Thailand.*
**Corresponding author:* Nattachote Rugthaicharoencheep; Phone: +66 61-353-6426; Email: nattachote.r@rmutp.ac.th.

program (FEA) was used to simulation in this study. Study was compared the characteristics of insulation suspension due to insulation failure [5]. In 2016 Att Phayomhom, and others analyzed the public's EMF exposure limits caused by different arrangements of 69 kV and 115 kV conductors. Analyze EMF values with Microsoft Excel and present the analysis results graphically with MATLAB program. [6]. In 2017 Pramuk Unahalekhaka and Karun Sirichunchuen studied the case of a lightning strike on the top and side wires of 56/57-2 TIS. 1251 piles type and 57-2 TIS. 1077 line poles type. This study simulated the electric field distribution along the insulator. This study used FEA and ATP-EMTP program. The model uses 10/350µs lightning surge currents of 20 kA, 40 kA, and 80 kA, respectively [7].

Therefore, this paper present determination of electric field stress from ozone gas generating electrodes for clean rooms.

THEORY OF ANALYZING THE ELECTRIC FIELD THAT AIR IONIZATION THE ELECTRODE ASSEMBLY

In data storage papers, it is recommended to primarily use SI (MKS) units, with English units provided as secondary units in parentheses when necessary. For instance, express data density is shown as “15 Gb/cm2 (100 Gb/in2)”. Exceptions are allowed when English units are used as trade identifiers, such as “3½ -in disk drive”. It's important to avoid the combination of SI and CGS units, such as using amperes for current and CGS units for magnetic fields. The definition of electric field stress (E) is density of electric flux (D) [8]-[9].

$$E= \frac{D}{\varepsilon} \tag{1}$$

$$\varepsilon= \varepsilon_r \varepsilon_0 \tag{2}$$

where ε_0 is free space of permittivity
ε_r is permittivity relative

Electric field generated by the electrode is non-uniform. This electrode type subjects each point within the electric field to varying degrees of strain, influenced by the electrode's geometry, resulting in an uneven electric field distribution, as depicted in the Figure 2. [3], [10]-[11].

The highest electric field stress is experienced at the surface of the spherical electrode and can be calculated as follows:

$$E_{max}= \frac{U}{d\eta^*} \tag{3}$$

Corona discharge is a high-voltage phenomenon that occurs on the surface of conductors or electrical components, typically resulting in energy losses within power systems. This process transforms electrical energy into various forms such as heat, light, sound, electromagnetic waves, and chemical byproducts. When a substantial voltage difference exists between electrodes, it initiates high-frequency acoustic emissions—a process associated with gas ionization and the formation of substances like ozone and nitrogen oxides. As the voltage continues to increase, small violet-colored glows begin to emerge along the conductor’s surface, marking the visual onset of corona discharge. This effect not only signifies energy dissipation but also introduces electromagnetic disturbances that can interfere with radio communication. In extreme conditions, excessive voltage levels can trigger arcing or flashovers, collectively referred to as corona effects [12]-[13].

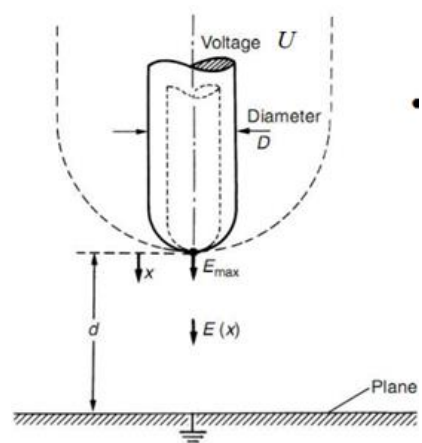

Fig. 2. The distribution of electric field.

The dissociation of air begins when the applied voltage reaches the Disruptive Critical Voltage—the minimum threshold necessary to initiate this process. At this stage, the electric field strength becomes sufficient to energize free electrons present in the air, significantly increasing their kinetic energy. These energized electrons then collide with surrounding gas molecules, resulting in ionization and the release of additional free electrons and ions. This chain reaction gives rise to an audible sound phenomenon, even in the absence of visible light emissions [14]–[15].

The technique of numerical employed for dividing the domain into smaller subsections known as elements is called "The finite element method", typically in the form of squares or triangles, as demonstrated in Figure 3. This method is widely utilized for engineering problem analysis and is a valuable tool for the solution of differential equations. It finds application across various fields, including solid mechanics, enabling the analysis of changes in shape and stress within mechanical components such as aircraft structures, buildings, bridges, and other complex structures. Regardless of whether the materials involved exhibit elasticity, plasticity, or elongation, the finite element method proves to be a versatile tool. It is utilized for addressing a broad spectrum of static and dynamic problems, as well as for conducting analyses of fluid flow, heat transfer, mass transfer, and more. In a basic analysis of typical mechanical structures or components, equations expressing the relationships we aim to understand, such as displacement at any point within a component, are derived based on differential equations. These outcomes are termed exact solutions. However, many machines and structures exhibit complex shapes, characterized by concave sections, various curves, and irregular cross-sectional areas. Additionally, certain areas may experience abrupt changes in loads or involve the use of diverse materials. Consequently, obtaining straightforward solutions using ordinary or partial differential equations is challenged in such cases. In these situations, systems of algebraic equations are resorted to as an alternative to solving differential equations [2], [16].

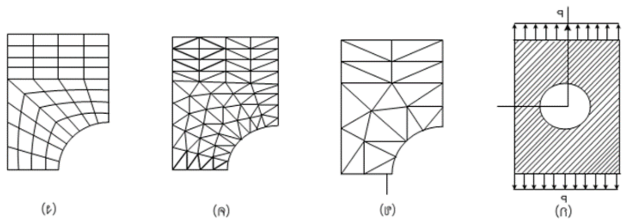

Fig. 3. Subdivisions of various elements within a material.

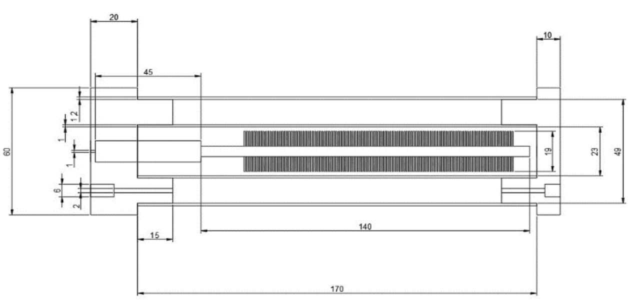

Fig. 4. Model of the 1 mm. bristle electrode.

The approach discussed here implies that for each element, the solution must inherently align with the governing equation. In the Finite Element Method (FEM), this principle serves as the foundational concept, where an equation is formulated for each element to correspond to the specific differential equation relevant to the problem at hand. These individual element equations are then aggregated into a comprehensive system of equations, analogous to assembling various pieces to construct an overall representation of the real-world problem. Solving these equations yields approximate results at various points within the problem's domain. The accuracy of these calculated approximations hinges on factors such as the size and number of elements used for problem-solving and the underlying assumptions guiding the internal interpolation functions applied to each element. These internal interpolation functions can take on diverse forms, including linear distribution. For instance, in a triangular element with corner temperatures of 30, 40, and 50 degrees Celsius, a linear interpolation function approximates temperatures at different locations within the element [2], [11]. Model of the 1 mm. bristle electrode is depicted in Fig. 4.

Fig. 4. shows the width of the electrode is 1 mm. Model of the 2 mm. bristle electrode is depicted in Fig. 5.

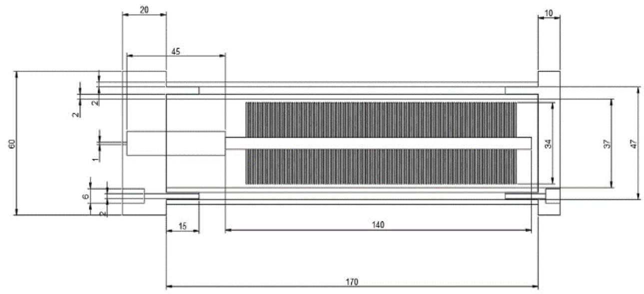

Fig. 5. Model of the 2 mm bristle electrode.

Fig. 5. shows the width of the electrode is 2 mm. Model of the 2.5 mm. bristle electrode is depicted in Fig. 6.

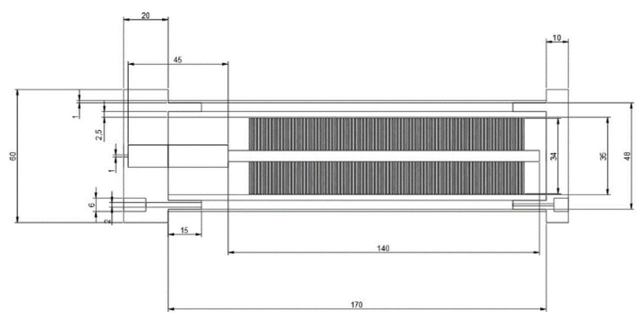

Fig. 6. Model of the 2.5 mm bristle electrode.

Fig. 6. shows the width of the electrode is 2.5 mm. The material component image displaying metal part is depicted in Fig. 7.

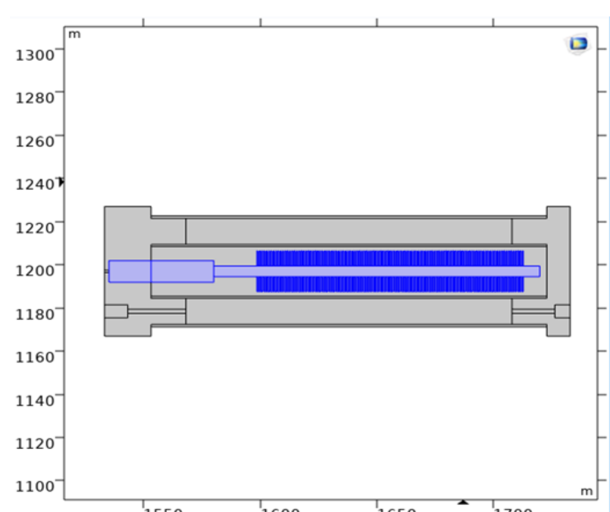

Fig. 7. The material component image displaying metal part.

The air part is depicted in Fig. 8.

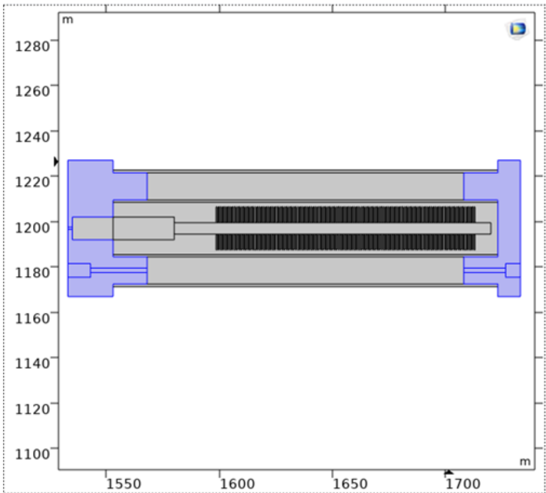

Fig. 8. The air part.

The glass material is depicted in Fig. 9.

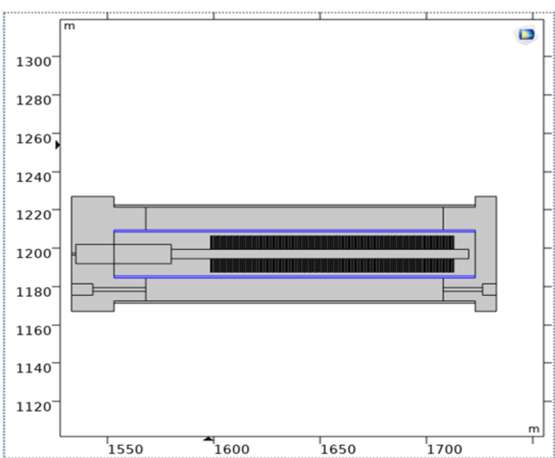

Fig. 9. The glass material.

The stainless steel pipe is depicted in Fig. 10.

The results of electric field analysis with Comsol software.

Calculated analysis results for the right bar: Red for the maximum and Blue for 1 mm. is depicted in Fig. 12.

The results analysis of electric field stress potential distribution at 1 mm. is depicted in Fig. 13.

Calculated analysis results for the right bar: Red for the maximum and Blue for 2 mm. is depicted in Fig. 14.

The results analysis of electric field stress potential distribution at 2 mm. is depicted in Fig. 15.

Calculated analysis results for the right bar: Red for the maximum and Blue for 2.5 mm. is depicted in Fig. 16.

The results analysis of electric field stress potential distribution at 2.5 mm. is depicted in Fig. 17.

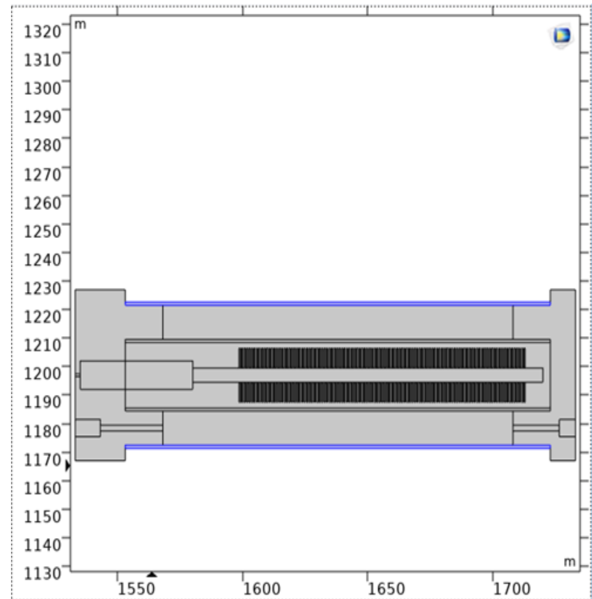

Fig. 10. The stainless steel pipe.

The Teflon material part is depicted in Fig. 11.

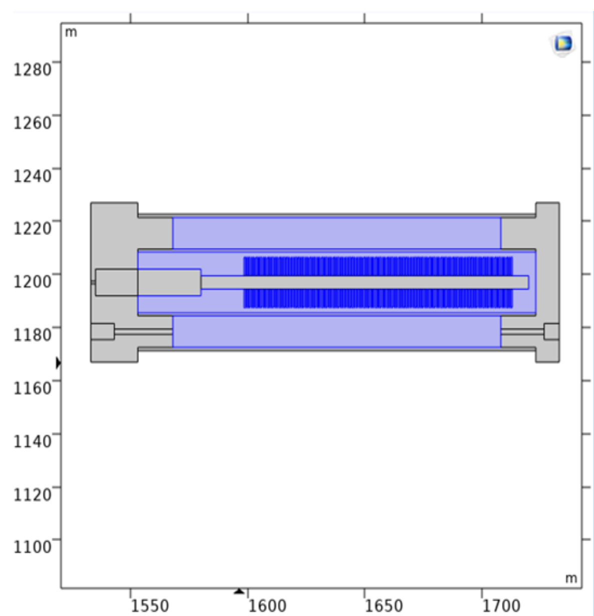

Fig. 11. The Teflon material part.

In this study, variables are being determined from real specimens used in the test to assess ozone degradation. The assembly of a test kit is display in Figure 18. The assessment takes into account variations in electrode characteristics and factors influencing the ionization of gas molecules within the test kits. These variations and transitions are then compared with samples of electric fields as part of the analysis [17]-[18].

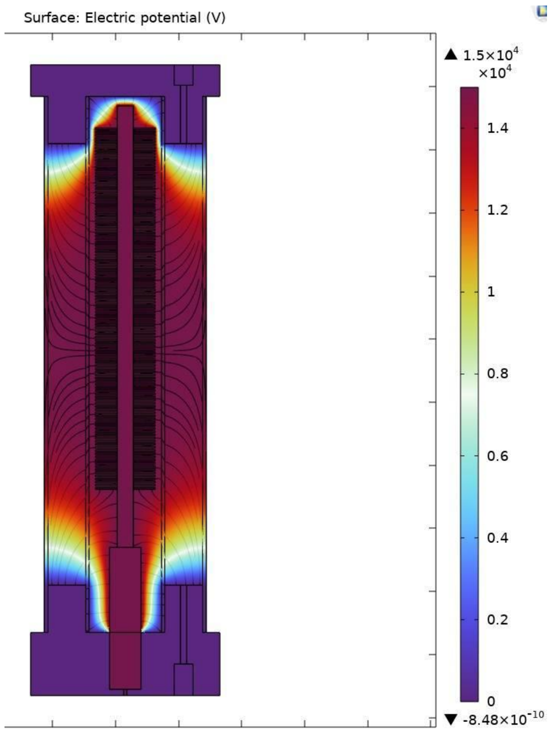

Fig. 12. Calculated analysis results for the right bar: Red for the maximum and Blue for 1 mm.

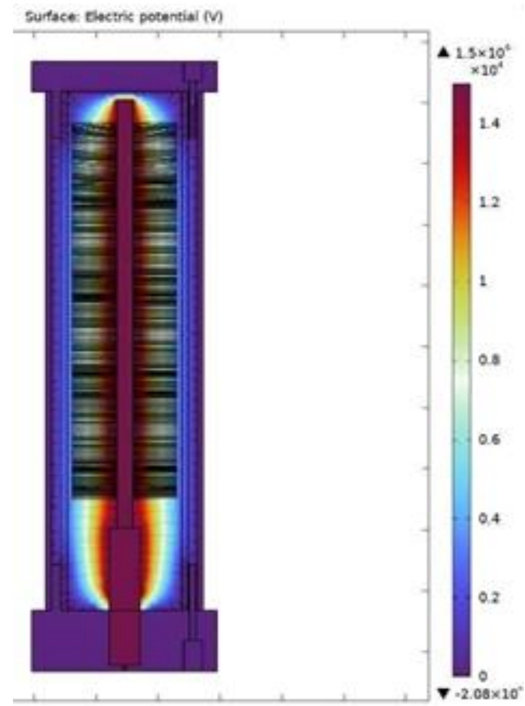

Fig. 14. Calculated analysis results for the right bar: Red for the maximum and Blue for 2 mm.

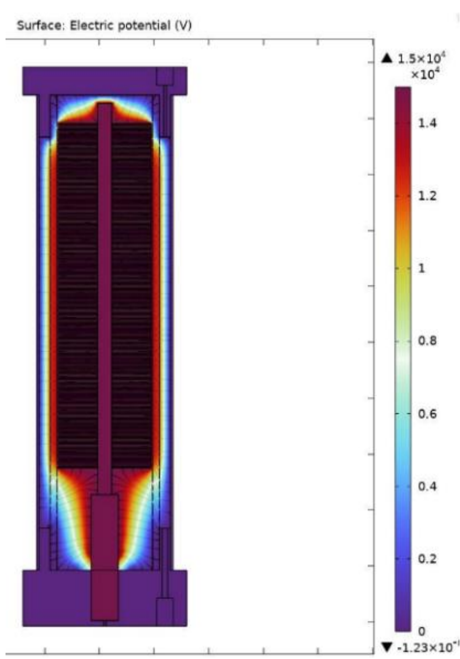

Fig. 13. The results analysis of electric field stress potential distribution at 1 mm.

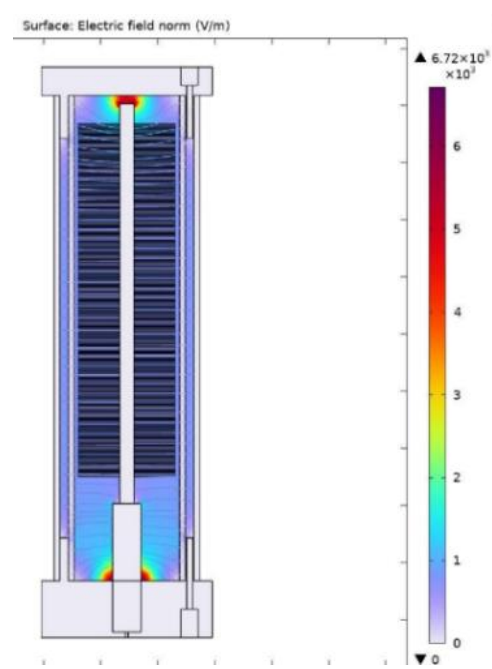

Fig. 15. The results analysis of electric field stress potential distribution at 2 mm.

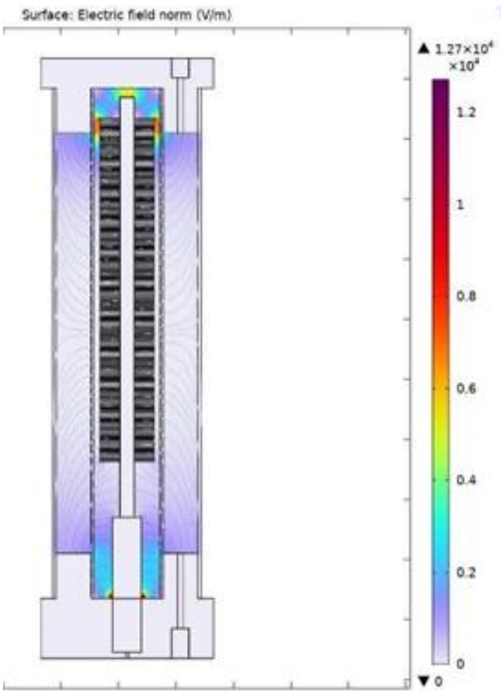

Fig. 16. Calculated analysis results for the right bar: Red for the maximum and Blue for 2.5 mm.

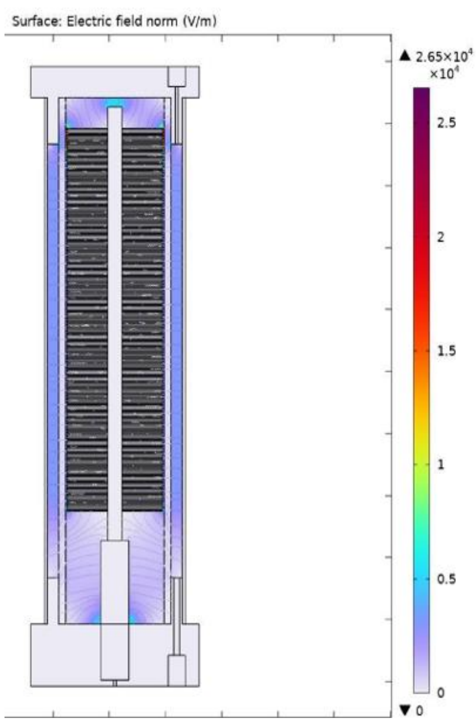

Fig. 17. The results analysis of electric field stress potential distribution at 2.5 mm.

Fig. 18. Assembly of a test kit for installation on stainless steel tubes and glass tubes inside, which together constitute the dielectric layer.

Expanding upon the previously discussed formulation of the operational process, the comparison is currently being undertaken. In this context, the simulation results obtained in this project, utilizing wire bristle electrodes, are being compared with the results of earlier experimental simulations involving pointed electrodes as illustrated in Fig. 19. The outcomes indicate that the simulation results in this project are characterized by a notably higher electric potential in comparison to the previous experiments [19]-[20].

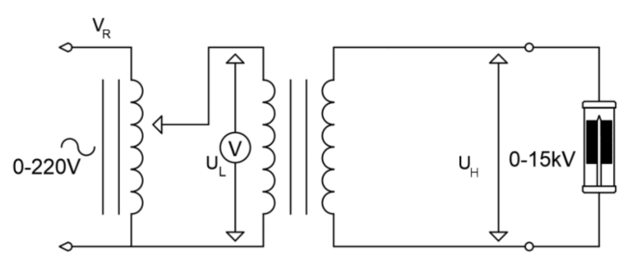

Fig. 19. Electrode unit test circuit in high voltage.

3. ANALYSIS AND RESULTS

Ozone determination is conducted using a spectrophotometer by placing a sample of distilled water that has been sprayed with ozone gas into a cuvette. This cuvette is then positioned inside a test chamber for measurement. Ozone determination with spectrophotometer is depicted in Fig. 20. [2], [16].

Fig. 20. Ozone determination with spectrophotometer.

Fig. 20. spectrophotometer is a water quality meter based on the principles of light transmission and absorption. The machine uses UV-Vis Spectroscopy technique. Measure the amount of light and intensity or light intensity in the UV to white light range. Spectrophotometer display: Red channel (wavelength range in nm); Green line ozone concentration is depicted in Fig. 21.

Fig. 21. Spectrophotometer display: Red channel (wavelength range in nm); Green line ozone concentration.

Fig. 21. Shows wavelength range is 212.0 nm, 215.0 nm, 225 nm, 233 nm, 241.0 nm, 259 nm, 280 nm, and 288 nm, respectively. Abs is -0.574, -0.352, -0.719, -0.791, -0.749, -0.701, -0.696, and -0.676, respectively.

The anthracite coal consists of 5 blended ratios. The 0 percent, 25 percent, 50 percent, 75 percent, and 100 percent is sub-bituminous [15]-[16] Results for electrodes with a 1 mm dielectric thickness is depicted in Table 1.

Table 1. Results for electrodes with a 1 mm dielectric thickness

Voltage (V)	High Voltage (kV)	The amount of gas Ozone concentration (g./l./hr.)	Std (ppm)
20	1.36	191	1.21E+07
60	4.09	873	5.51E+07
00	6.82	1,147	3.39E+08
140	9.54	1,639	1.92E+08
180	12.27	1,867	5.71E+08
220	15	2,170	3.13E+08

Table 1. shows voltage 20 V the amount of gas ozone concentration is 191 g./l./hr., voltage 60 V the amount of gas ozone concentration is 873 g./l./hr., voltage 100 V the amount of gas ozone concentration is 1,147 g./l./hr., voltage 140 V the amount of gas ozone concentration is 1,639 g./l./hr., voltage 180 V the amount of gas ozone concentration is 1,867 g./l./hr., and voltage 220 V the amount of gas ozone concentration is 2,170 g./l./hr.,

A graph illustrating ozone production at various electrode pressures, featuring a 1 mm dielectric thickness is depicted in Fig. 22.

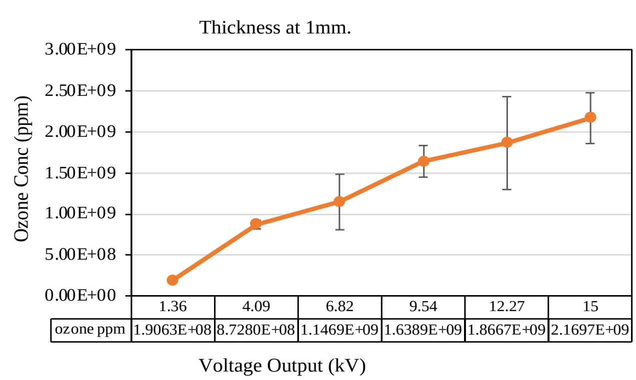

Fig. 22. A graph illustrating ozone production at various electrode pressures, featuring a 1 mm dielectric thickness.

Fig. 22. shows voltage output is 1.36 kV. ozone is 1.9063E+08 ppm. Voltage output 4.09 kV ozone is 8.728E+08 ppm. Voltage output 6.82 kV ozone is 1.1469E+09 ppm. Voltage output 9.54 kV ozone is 1.6389E+09 ppm. Voltage output 12.27 kV ozone is 1.8667E+09 ppm. Voltage output 15.00 kV ozone is 2.1697E+09 ppm.

Results for electrodes with a 2 mm dielectric thickness is depicted in Table 2.

Table 2. Results for electrodes with a 2 mm dielectric thickness

Voltage (V)	High Voltage (kV)	The amount of gas Ozone concentration (g./l./hr.)	Std (ppm)
20	1.36	1,245	1.24E+08
60	4.09	1,279	1.28E+08
100	6.82	1,671	1.67E+08
140	9.54	1,736	1.74E+08
180	12.27	2,068	2.07E+08
220	15	2,340	2.34E+08

Electric Field Maximum 220V=15kV

Table 2. shows voltage 20 V the amount of gas ozone concentration is 1,245 g./l./hr., voltage 60 V the amount of gas ozone concentration is 1,279 g./l./hr., voltage 100 V the amount of gas ozone concentration is 1,671 g./l./hr., voltage 140 V the amount of gas ozone concentration is 1,736 g./l./hr., voltage 180 V the amount of gas ozone concentration is 2,068 g./l./hr., and voltage 220 V the amount of gas ozone concentration is 2,340 g./l./hr.,

A graph illustrating ozone production at various electrode pressures, featuring a 2 mm dielectric thickness is depicted in Fig. 23.

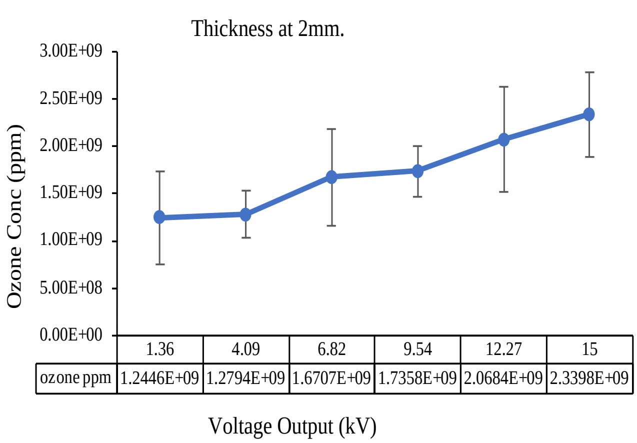

Fig. 23. A graph illustrating ozone production at various electrode pressures, featuring a 2 mm dielectric thickness.

Fig. 23. shows voltage output is 1.36 kV. ozone is 1.2446E+09 ppm. Voltage output 4.09 kV ozone is 1.2794E+09 ppm. Voltage output 6.82 kV ozone is 1.6707E+09 ppm. Voltage output 9.54 kV ozone is 1.7358E+09 ppm. Voltage output 12.27 kV ozone is 2.0684E+09 ppm. Voltage output 15.00 kV ozone is 2.3398E+09 ppm.

Results for electrodes with a 2.5 mm dielectric thickness is depicted in Table 3.

Table 3. Results for electrodes with a 2.5 mm dielectric thickness

Voltage (V)	High Voltage (kV)	The amount of gas Ozone concentration (g./l./hr.)	Std (ppm)
20	1.36	1,409	1.41E+08
60	4.09	1,564	1.56E+08
100	6.82	1,647	1.65E+08
140	9.54	1,687	1.69E+08
180	12.27	1,778	1.78E+08
220	15	2,600	2.60E+08

Table 3. shows voltage 20 V the amount of gas ozone concentration is 1,409 g./l./hr., voltage 60 V the amount of gas ozone concentration is 1,564 g./l./hr., voltage 100 V the amount of gas ozone concentration is 1,647 g./l./hr., voltage 140 V the amount of gas ozone concentration is 1,687 g./l./hr., voltage 180 V the amount of gas ozone concentration is 1,778 g./l./hr., and voltage 220 V the amount of gas ozone concentration is 2,600 g./l./hr.,

A graph illustrating ozone production at various electrode pressures, featuring a 2.5 mm dielectric thickness is depicted in Fig. 24.

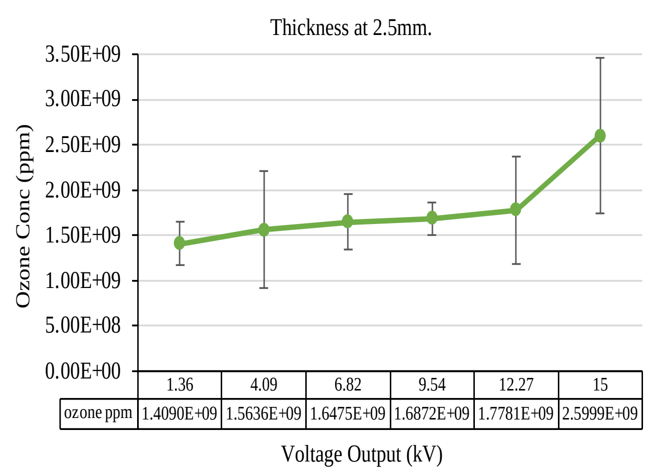

Fig. 24. A graph illustrating ozone production at various electrode pressures, featuring a 2.5 mm dielectric thickness.

Fig. 24. shows voltage output is 1.36 kV. ozone is 1.4090E+09 ppm. Voltage output 4.09 kV ozone is 1.5636E+09 ppm. Voltage output 6.82 kV ozone is 1.6475E+09 ppm. Voltage output 9.54 kV ozone is 1.6872E+09 ppm. Voltage output 12.27 kV ozone is 1.7781E+09 ppm. Voltage output 15.00 kV ozone is 2.5999E+09 ppm.

The results compare std and voltage 3 sizes of electrodes is depicted in Fig. 25.

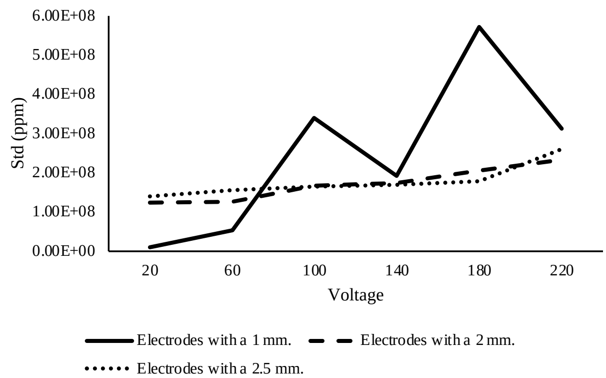

Fig. 25. The results compare std and voltage 3 sizes of electrodes.

Fig. 25. shows voltage output is 20 V. Ozone of electrode 2 mm. and 2.5 mm. is higher than 1 mm. 1.12E+08 ppm, and 1.29E+08 ppm, respectively. Voltage output is 60 V. Ozone of electrode 2 mm. and 2.5 mm. is higher than 1 mm. 7.29E+07 ppm, and 1.01E+08 ppm, respectively. Voltage output is 100 V. Ozone of electrode 2 mm. and 2.5 mm. is lower than 1 mm. 1.72E+08 ppm, and 1.74E+08 ppm, respectively. Voltage output is 140 V. Ozone of electrode 2 mm. and 2.5 mm. is lower than 1 mm. 1.80E+07 ppm, and 2.30E+07 ppm, respectively. Voltage output is 180 V. Ozone of electrode 2 mm. and 2.5 mm. is lower than 1 mm. 3.64E+08 ppm, and 3.93E+08 ppm, respectively. Voltage output is 220 V. Ozone of electrode 2 mm. and 2.5 mm. is lower than 1 mm. 7.90E+07 ppm, and 5.30E+07 ppm, respectively.

4. CONCLUSION

The test results of this study found that ozone content is affected by the thickness of the glass tube employed in the workpiece, leading to variations depending on pressure levels. Improved ozone production is evident when workpieces utilize a 2mm thick glass tube, especially at lower pressures, with minimal variation within the 20 – 60V voltage range. However, as the voltage range reaches 100V, divergent results become apparent. To increase ozone production, voltage should be incrementally raised in 80V increments. Conversely, in the case of specimens using 2.5 mm thick glass tubes, superior ozone production is noted at lower voltage levels, but the increase in pressure does not significantly augment ozone production, with the exception of the 220V voltage level, which surpasses other voltage levels.

ACKNOWLEDGEMENTS

The authors would like to thank the support from Department of Electrical Engineering, Faculty of Engineering, Rajamangala University of Technology Phra Nakhon to fund research and tools for research analysis and co-author thank for all.

REFERENCES

[1] Y. Premjit, N. U. Sruthi, R. Pandiselvam, and A. Kothakota, “Aqueous ozone: Chemistry, physiochemical properties, microbial inactivation, factors influencing antimicrobial effectiveness, and application in food,” *Comprehensive Reviews in Food Science and Food Safety*, vol. 21, issue 2, pp.1054-1085, 2022.

[2] E. Kuffel, W.S. Zaengl, and J. Kuffel, *High Voltage Engineering:Fundamentals*, Newness, Oxford, pp. 50-74, 2000.

[3] Australian Standard, AS2947.1-1989, Insulators porcelain and glass for overhead power lines voltage greater than 1000 V-A. C Part I: Test methods.

[4] T. Lantharthong, and S. Nedphokaew, “Analysis of Electric field and Modeling Design of High Voltage Cable terminators for PD Testing Using SF_6 Insulator”, International Conference on Electrical Engineering 2008 (ICEE 2008), 2008.

[5] P. Unahalekhaka, and S. Phonkaphon, “Simulation of Potential and Electric Field Due to Defective Insulator in 115 kV Transmission Line,” *GMSARN Int. J.*, vol. 8, no. 1, pp. 7-12, 2014.

[6] A. Phayomhom, T. Kasirawat, S. Phontusa, J. Halapee, B. Ainsuk, K. Kveeyarn, N. Rugthaicharoencheep, and A. Puttarach, “Analysis of Electric Field and Magnetic Field from Overhead Subtransmission Lines Affecting Occupational,” *GMSARN Int. J.*, vol. 10, no. 1, pp. 25-32, 2016.

[7] P. Unahalekhaka, and K. Sirichunchuen, “Influence of Electric Field Distribution along the Line Post and Pin Post Insulator due to Lightning Strike,” *GMSARN International Journal*, Vol. 11, No. 1, pp. 23-27, 2017.

[8] IEC Publication No.156, “Method for the determination of the electric strength of insulating Oil”, 1994.

[9] Li Naiyi, Peng Zongren, Liu Peng, “Electric field simulation and analysis of 1100 kV DC SF6 gas-insulated wall bushing,” High Voltage Engineering, vol. 46, pp. 205-214, 2020.

[10] IEC Publ. 383-1983, “Test on insulators of ceramic material or glass for overhead lines with a nominal voltage greater than 1000 V,” 1983.

[11] IEC Publ.1211-1994, “Insulators of ceramic material or glass for overhead lines with a nominal voltage greater than 1000 V-puncture testing,”

[12] Y. Jiye, Y. Xiaozheng, M. Qiang, C. Xi, C. Baoqi, and L. Mingyue, “Three dimensional simulation of bushing electric field distribution of ± 800 kV converter transformer,” *Hydropower Energy Sci.*, 36, pp. 188-191, 2018.

[13] S. O’Keeffe, C. Fitzpatrick, and E. Lewis, “An optical fibre based ultra violet and visible absorption spectroscopy system for ozone concentration monitoring,” Sensors and Actuators B: Chemical, vol. 125, issue 2, pp. 372-378, 2007.

[14] S. Nedphograw, HighVoltage Engineering Book, 2008, ISBN 978-974-0667-91-9.

[15] IEC Publication No.60-2 “High Voltage test techniqued Part 2: Measuring Systems”,1994.

[16] Diesendorf. W., Insulation Co-ordination in High Voltage Electric Power Systems, Butterworth & Co., Ltd., pp.47-48, 1974.

[17] Stanley BT, 1999, Feedgas for Modern High-Performance Ozone Generators Ozonia Ltd, Duebendorf Switzerland.

[18] Nur M, Resti M, Arianto F, Muhlisin Z, Teke S, Susan A I, Winarni TA, Susilo and Muharam H., “Power analysis of ozone generator for high capacity production,” 2014 International Symposium on Technology Management and Emerging Technologies (ISTMET), 2014.

[19] E. Volpov, "Electric field modeling and field formation mechanism in HVDC SF_6 gas insulated systems," IEEE Transactions on Dielectrics and Electrical Insulation, vol. 10, issue 2, pp. 204-215, 2003.
[20] Z. Shiling, and P. Zongren, "Application of Finite Element Method to Three-dimensional Electric Field Computer-aided Simulation of UHV Wall Bushing," 2019 6th International Conference on Information Science and Control Engineering (ICISCE), pp. 159-163, doi: 10.1109/ICISCE48695.2019.00041.